Visibility Analysis for Assembly Fixture Calibration Using Screen Space Transformation

Zhenyu Kong
Dimensional Control Systems, Inc.,
Troy, MI 48084
e-mail: jkong@3dcs.com

Wenzhen Huang
e-mail: huang@cae.wisc.edu

Dariusz Ceglarek
e-mail: darek@engr.wisc.edu

Department of Industrial Engineering,
University of Wisconsin-Madison,
Madison, WI 53706

In a number of manufacturing processes—tooling installation, calibration, and maintenance—guarantee the precision of fixtures and play important roles toward the overall quality of products. Recently, a new type of measurement equipment called a "laser tracker" was developed and utilized for assembly fixture calibration to shorten calibration time and improve the accuracy of the currently used theodolite systems. Though calibration of the assembly fixture is critical for product quality, as such, calibration time creates a significant burden for productivity of multistation assembly processes. In order to shorten calibration lead time, the number of necessary setups, determined by visibility analysis, needs to be minimized. This paper presents a screen space transformation-based visibility analysis that allows minimizing the number of setups. The screen space transformation is applied to transform the visibility problem from three- to two-dimensional space, thus, efficiently solving the visibility problem. A case study illustrates the procedure and verifies the validity of the proposed methodology. This methodology can be applied not only for manufacturing processes, such as in-line fixture calibration, but also toward analysis and optimization of AGVs, robot navigation systems, and building security. [DOI: 10.1115/1.1947209]

Keywords: Visibility, Fixture Calibration, Screen Space Transformation

1 Introduction

1.1 Motivation. Dimensional control in multistation assembly processes has a significant impact on overall product quality and performance as well as on productivity and production cost. For example, two-thirds of engineering changes in automotive and aerospace industries are caused by dimensional faults, and about two-thirds of dimensional faults are caused by fixture failures [1,2]. The fixture-related dimensional faults during various production phases of a new product constitute up to 40% of all dimensional failures during preproduction, up to 70% during launch, and between 70 and 100% during one and two shifts of production, respectively [2]. A significant number of fixture-related failures are related to installation and maintenance. For example, during the phases of preproduction, launch, one, and two shifts of full production, about 25, 40, 100, and 52% of the fixture-related faults are caused by discrepancies in fixture installation and maintenance. From these data we can see that accurate fixture installation and maintenance are critical for the purposes of overall product quality. On the one hand, the overall importance of dimensional variation in manufacturing processes is reflected by extensive research focused on (i) shortened ramp-up and/or launch of new products by dimensional variation faults root-cause diagnostics [3–9], (ii) rapid fixturing deployment [10,11], and (iii) by optimal sensor placement [12–15]. On the other hand, however, there is a paucity of research related to fixture calibration and setup.

One of the most critical tasks in tooling installation and maintenance is fixture calibration, which guarantees the spatial accuracy of all tooling elements, such as locators, NC blocks, and clamps. The accuracy and precision in spatial position and orientation of all tooling elements in the fixture significantly affect the dimensional quality of parts. In general, calibration of each tooling element can be described as the determination of x, y, and z coordinates of a single or multiple points (features) located on the tooling element [16]. It is a common practice in the industry that the design nominal x, y, and z coordinates of the trihedral points are marked on the numerically controlled (NC) blocks when the blocks are being fabricated. Tooling calibration (certification) is the process of verifying that the positions of all tooling elements are within the design specification limits. Tooling fixtures are certified after tooling installation is completed [17]. Because of this constraint, fixture calibration must often be performed as an in-line operation, i.e., the fixture is not removed from the production line during calibration operations. Therefore, in this paper we will call it in-line fixture calibration, which is different from off-line fixture calibration where the fixture is taken off-line to other places, for example, the coordinate-measuring-machine (CMM) room, to perform necessary calibration measurements. In general, in-line fixture calibration is more challenging than off-line calibration since it needs to be done very rapidly to shorten production downtime. However, the rapid in-line fixture calibration is a challenging task because of the lack of ability to reposition or reorient fixtures and because of the complex environment surrounding the calibrated fixture (existing obstacles that limit visibility and accessibility to the calibrated fixture).

Currently, theodolite systems (Fig. 1) are widely used for fixture calibration in the automotive and aerospace industries [17]. A theodolite system for tooling calibration usually includes two heads, and the calibration procedure for each tooling element is based on the triangulation principle. However, currently used theodolite-based calibration systems have the following limitations: relatively complex setup procedures, low precision, operator dependence, and low efficiency.

A partial response to overcome the aforementioned challenges has led to the development of new measurement equipment, the "laser tracker" (Fig. 2), a system that requires a single head instead of two-heads [18], thus, improving visibility of tooling elements in the calibrated fixture. The laser tracker uses the laser beam and interferometry principle to measure distance from the target point. It can be used in a number of applications, such as

Contributed by the Manufacturing Engineering Division for publication in the ASME Journal of Manufacturing Science and Engineering. Manuscript received July 23, 2003; final revision received June 14, 2004. Associate Editor: E. C. De Meter.

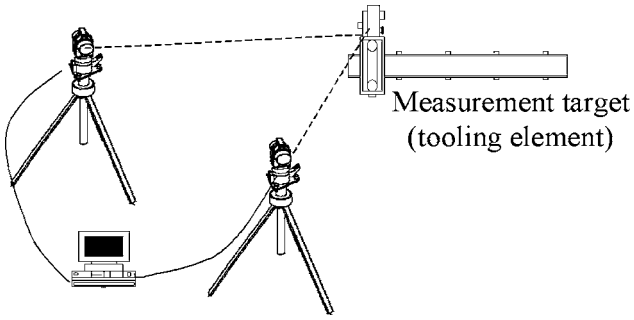

Fig. 1 Two-head theodolite system

tooling and robot calibration, surface contour measurement, or creation of error map for tool or probe positions of machine tools and CMMs, respectively. It enables a quicker setup, involving only one device. Moreover, it has precision at 0.01–0.2 mm in a normal production environment [18,19]. Additionally, the laser tracker measurement results are independent of operator skills and eyesight strength. All of the aforementioned characteristics of the laser tracker provide greater opportunities for application in tooling calibration. However, currently we lack a methodology to determine positions of the laser tracker system to be able to fully calibrate a given fixture or to determine the minimum number of necessary system setups.

The objective of this paper is to overcome the aforementioned challenges by developing a visibility analysis methodology for fixture calibration using screen space transformation (SST). The presented methodology simplifies the visibility problem by first transforming three-dimensional (3D) cases into two-dimensional (2D) cases and then conducting the necessary computational operations. The developed methodology increases the number of tooling elements visible from a single location of the calibration system, thereby, reducing the number of calibration setups and overall calibration time and improving accuracy and precision of fixture calibration.

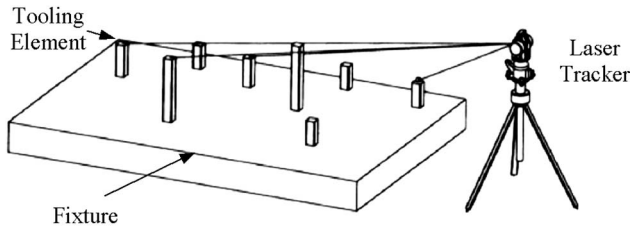

Fig. 2 Application of the laser tracker in large fixture measurement (API Inc.)

1.2 Related Work. Research related to visibility and accessibility can be classified into (i) generic methods and (ii) their applications for workpiece setups (machining processes, CMM inspections) or for measurement system setups (fixture calibrations using theodolite or laser tracker systems) (Table 1).

1.2.1 Accessibility and Visibility. Spyridi and Requicha [20] developed an analytical accessibility analysis method based on the concept of accessibility cones that can be computed using Gaussian images and Minkowski sums. The method was applied for workpiece inspection by coordinate measuring machines to determine if measured workpiece features can be reached by the CMM probe without collisions. Spitz et al. [21] and Spitz and Requicha [22] enhanced computational efficiency of the method by discretizing the workpiece and developing a graphic rendering methodology. Chen and Woo [23] and Woo [24] first developed the concept of a visibility map and provided a geometric algorithm to compute the visibility of part features to be inspected by CMMs.

1.2.2 Application of Accessibility-Visibility Methods. Accessibility-visibility methods were used in a number of applications to determine: workpiece setups in machining and CMM inspection and measurement system setups during tooling calibration (Table 1). Chen and Woo [23] and Woo [24] applied visibility maps to minimize the number of workpiece setups in computer numerically controlled (CNC) machining and CMM inspection. Wuerger and Gadh [25] applied visibility maps to compute the die-opening directions for removing fabricated workpieces. Yin and Xiong [26] applied visibility cones to identify obstacles modeled by using configuration space (C-Space) for mold parting, workpiece setup in NC-machining and CMM inspections.

The aforementioned applications focused on setups that can be characterized as identifying workpiece orientations to maximize visibility of all selected part features. Each necessary workpiece orientation is defined as a new setup, and the overall direction is classified in Table 1 as workpiece focused.

On the other hand, in tooling (fixture) calibration, the position and orientation of tooling are fixed, and thus, the problem is related to identifying measurement system position and orientation (setup) as a function of obstacles located in the environment. This overall direction is classified in Table 1 as environment focused. The goal of this direction is to identify positions from which the measurement equipment can measure all the targets (tooling elements) without being blocked by any obstacles in the environment. Chen et al. [17] developed a methodology for fixture cali-

Table 1 Related work on accessibility and visibility

		Applications	
	Accessibility and Visibility Methods	Minimizing number of workpiece setups	Minimizing number of measurement device setups
Workpiece focused: Orientation of workpiece to conduct measurement or machining (global/local visibility cone or visibility maps)	- *Accessibility cone* Spyridi and Requicha [20]; Spitz et al. [21]; Spitz and Requicha [22]; -Visibility maps Chen and Woo [23]; - *Visibility map and visibility matrix* (presented in this paper)	- *Machining* Chen and Woo [23]; Woo [24]; - *CMM* Wuerger and Gadh [25]; Yin and Xiong [26];	N/A
Environment focused: Position of measurement system or tool to conduct calibration, measurement or other tasks		N/A	Multiple device systems based on *visibility maps* (theodolite) Chen et al. [17] Single device systems based on *screen space transformation* (laser tracker) (presented in this paper)

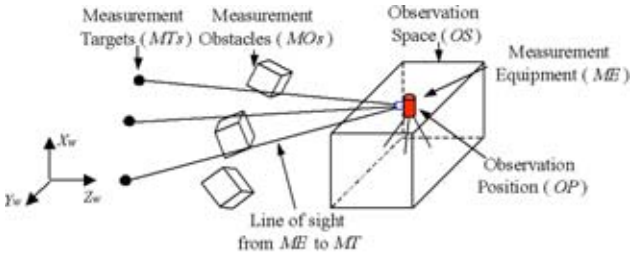

ME: Measurement Equipment. For example, laser tracker or theodolite.
MO: Measurement Obstacle. Any object between *ME* and *MT*.
MT: Measurement Target. For example, fixture locators/clamps.
OS : Observation Space. A workspace in which the *ME* is allocated.
OP : Observation Position. Any position inside the *OS*.

Fig. 3 Illustrations of visibility problem for in-line fixture calibration

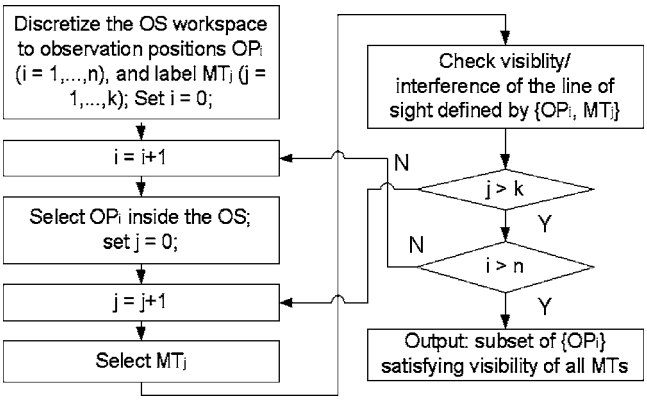

Fig. 4 Process of the direct visibility algorithm

bration based on the Gaussian sphere and visibility map. The method minimizes the number of needed setups of theodolites. However, the visibility algorithm based on the Gaussian sphere and visibility maps assumes that the "source of the visibility sight" (i.e., CMM probe, and/or tool in machining) can be moved in space with the same spatial orientation. This assumption is reasonable for applications such as visibility analysis of CMM inspections and NC machining operations. However, in the case of environment-focused applications, such as in-line fixture calibration, where the source of visibility sight is theodolite or the laser tracker system, the aforementioned assumption is not valid. Therefore, the Gaussian sphere-based visibility algorithm cannot be directly applied toward environment-focused applications.

1.3 Proposed Method. This paper presents a visibility method for environment-focused applications, such as in-line fixture calibration. The objective of the presented methodology is to minimize the number of setups of single-measurement equipment, such as the laser tracker. The presented methodology is based on the screen space transformation to transform 3D information about obstacles into 2D information, thus significantly simplifying computations. The proposed methodology is presented as a two-fold approach: (i) the screen space as well as homogeneous transformations are applied to transform objects from 3D to 2D space in which the visibility problem can be represented as 2D visibility maps (Sec. 3); (ii) simplified modeling of convex polyhedral obstacles is developed to significantly reduce the computational complexity (Sec. 4).

This paper is divided into six sections. Section 2 formulates the problem and provides motivation and the procedure for the screen space transformation. Then, Sec. 3 presents a visibility algorithm for tooling calibration using the screen space transformation to minimize the number of setups for measurement equipment. Section 4 provides a method that simplifies modeling of obstacles. A case study is presented to illustrate the proposed approach in Sec. 5. Finally, the methodology is summarized in Sec. 6.

2 Screen Space Transformation

2.1 Problem Statement. Figure 3 illustrates the environment-focused visibility problem as applied for in-line fixture calibration along with the corresponding terminology. Observation space (OS) is a predefined space in which the measurement equipment (ME) is allocated. Any position inside the OS is called an observation position (OP). Measurement targets (MTs) are those feature points of the tooling elements (locators and clamps) that need to be measured and calibrated by the ME. Any object that may block lines of sight between ME and MTs is called a measurement obstacle (MO), which cannot be removed during the process of fixture calibration. Examples of MOs are material handling device(s), robots, and other tooling elements obstructing lines of sight between the ME and the calibrated MT. A single ME setup is described as a single position of ME within the OS workspace selected for calibration of a given set of MTs. In case of in-line fixture calibration, each MT represents a single geometrical feature of a given tooling element (locator or clamps). For example, in the case of a NC block used as a locator, the geometrical feature used for calibration is the trihedral point.

The notion that a MT is visible signifies that the line of sight between ME and MT are not obstructed by any of the MOs. Otherwise, the MT is invisible and the ME needs another setup (position) to measure the MT. Therefore, for the environment-focused visibility problem, the objective is to identify the minimum number of OPs within the OS workspace such that all the MTs to be calibrated are visible from the selected OPs. Ideally, it is desirable to identify a single setup to calibrate all the MTs.

2.2 Direct Visibility Algorithm. In order to solve the problem of a minimum number of setups, the visibility should be checked for every MT and all the possible OPs within the OS workspace, as illustrated in Fig. 3.

Intuitively, this can be done by following the procedure shown in Fig. 4, called the direct visibility algorithm (DVA). This procedure is divided into three steps: (i) discretize the OS workspace to a set of feasible OP positions; (ii) check the visibility status of any line of sight defined between all feasible pairs of $\{OP_i, MT_j\}$, where OP_i $(i=1,2,\ldots,n)$ represents all possible OPs and MT_j $(j=1,2,\ldots,k)$ represents all selected MTs and; (iii) conduct combinatorial search for the smallest subset of OP_i $(i=1,2,\ldots,s)$, which satisfies visibility for all the MTs being calibrated.

The above procedure, though conceptually simple, is computationally extremely intensive in 3D space. The obstacles are 3D polyhedrons, which can be represented by a number of surface polygons. If m is the number of surface polygons that represent all the MOs, n refers to the number of discretized OPs within the OS, and k represents the number of MTs, then the complexity of this algorithm is $O(mnk)$. Each basic operation of the above procedure involves checking intersection between a straight line and a polygon in 3D space, which is computationally quite intensive.

2.3 Procedure of Screen Space Transformation. The direct visibility algorithm based on exhaustive search cannot be directly applied in industrial environment due to its extremely intensive computations that are related to (i) calculations of intersections between straight lines and planes in 3D space, and (ii) large number of surface polygons representing obstacles. In order to overcome the aforementioned challenges, the problem will be converted from 3D to 2D space by using the screen space transformation (SST).

Figure 5 illustrates the view space, which is the original 3D space without any transformation. All the objects are located in a world coordinate system (WCS), represented by *Xw Yw Zw*. For

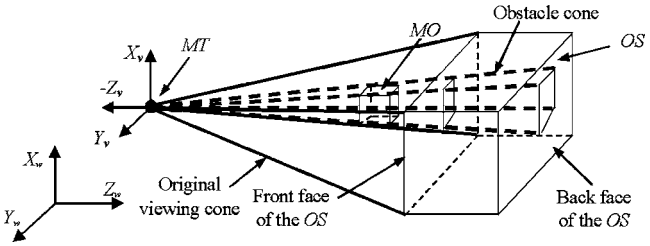

Fig. 5 Illustration of the view space

each MT, there is a local view coordinate system (LVCS), represented by *Xv Yv Zv*. We can see that the visibility problem is equivalent to taking each MT as sight source and identifying the visible OP positions within the OS. In Fig. 5 all the viewing orientations from the MT to the OS form a view cone that is called original viewing cone (represented by bold and solid lines), and the space occluded by the MO is also a cone, called the obstacle cone (represented by bold and dashed lines). For a given MT, all the OP positions, that are inside of the original view cone but outside of the obstacle cone are visible to the given MT.

The view space, as shown in Figs. 5 and 6(*a*), represents perspective projection, which requires heavy computations due to varying orientation for each line of sight. A SST [27] can be utilized to transform the 3D view space to a 2D screen space, where the original lines of sight become parallel to each other, and the perspective projection is converted to an orthogonal projection, as shown in Fig. 6(*b*). In an orthogonal projection z coordinates of all objects can be omitted, and thus the computation can be simplified to a 2D domain that is perpendicular to the projection orientation. Therefore, the original 3D view and obstacle cones become 2D polygons, and a line of sight is alleviated to a point. Consequently, the computation of intersection between a line of sight and an obstacle polygon in 3D space can be converted to verify if a point is within a polygon in 2D space.

Figure 7 describes the parameters of the SST in 3D and 2D views with an MT being selected as the origin of the local view coordinate system. For each MT (Xv, Yv, Zv), the front and back faces of the OS (Fig. 5) are utilized as near view plane, and far view plane, respectively, for the purpose of SST transformation. The local view coordinate system in 3D view space can be transformed to a screen space coordinate system by using the following SST transformation matrices

$$T_{\text{pers}} = T_{\text{pers2}} T_{\text{pers1}b} T_{\text{pers1}a} \tag{1}$$

where

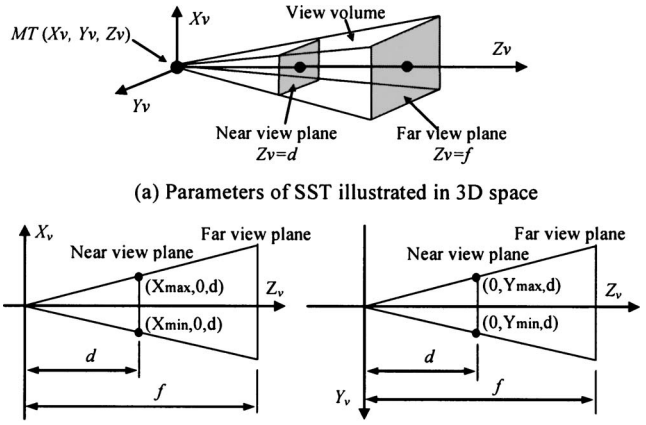

Fig. 7 Parameters of transformation from view space to screen space

$$T_{\text{pers1}a} = \begin{bmatrix} 1 & 0 & \dfrac{x_{\max} + x_{\min}}{2d} & 0 \\ 0 & 1 & \dfrac{y_{\max} + y_{\min}}{2d} & 0 \\ 0 & 0 & 1 & 0 \\ 0 & 0 & 0 & 1 \end{bmatrix},$$

$$T_{\text{pers1}b} = \begin{bmatrix} \dfrac{2d}{x_{\max} - x_{\min}} & 0 & 0 & 0 \\ 0 & \dfrac{2d}{y_{\max} - y_{\min}} & 0 & 0 \\ 0 & 0 & 1 & 0 \\ 0 & 0 & 0 & 1 \end{bmatrix}$$

and

$$T_{\text{pers2}} = \begin{bmatrix} 1 & 0 & 0 & 0 \\ 0 & 1 & 0 & 0 \\ 0 & 0 & f/(f-d) & -fd/(f-d) \\ 0 & 0 & 1 & 0 \end{bmatrix}$$

where all the parameters in the Eq. (1) are shown in Fig. 7.

It can be observed that screen space transformation has a side effect of distorting the back of the view volume in the screen space (Fig. 6(*b*)). However, this distortion causes errors during calculations of object volume only but not on the visibility (intersections) [27].

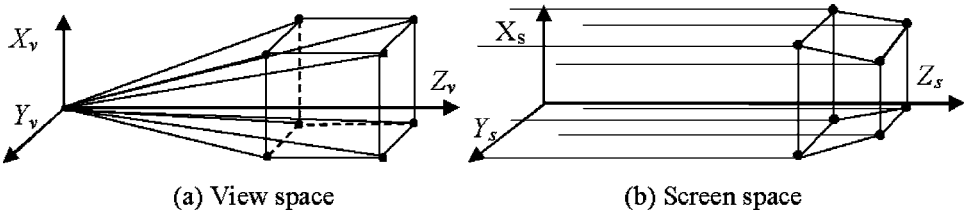

Fig. 6 View space and screen space

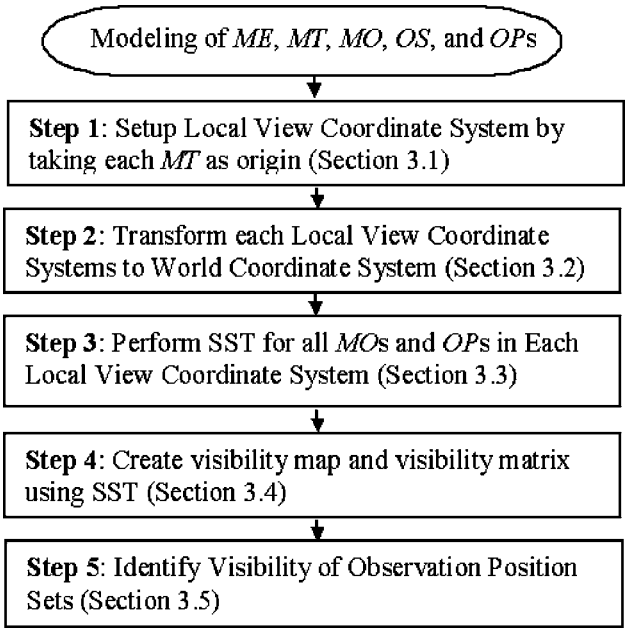

Fig. 8 Procedures of the SST-based visibility algorithm

3 Visibility Algorithm Using Screen Space Transformation

In this section, a visibility algorithm based on SST transformation is presented. Figure 8 shows the step-by-step procedure of the proposed visibility methodology with detailed explanations presented below.

3.1 Setup of Local View Coordinate System for Each Measurement Target. In this step, the local view coordinate systems that take each MT as origins are set up. For simplicity, each OS workspace is represented as a sphere. However, it does not impose any practical limitations because any given OS with different shapes can be easily transferred to a sphere(s) that contains it. Furthermore, the spherical shape representation of the OS workspace can lead to a convenient setup of local view coordinate system.

Figure 9 illustrates a simple example of the visibility problem for which the proposed visibility algorithm is applied. There are two MTs, one MO with cubic shape, and a spherical OS, which is discretized into a related number of OPs. Any general case can be expanded from this scenario by using the same procedure. As mentioned in Sec. 2, it is assumed that all MOs are convex polyhedrons (this assumption can be released since even if a MO is concave, it can be decomposed into a summation of convex polyhedrons).

Figure 10 illustrates two local view coordinate systems $LVCS_1$ and $LVCS_2$ taking MT_1 and MT_2 as origins, respectively. Because of the spherical shape of the OS, the orientation of the axis of each local view coordinate system can be determined conveniently. We use MT_1 as an example to explain how to obtain the orientation of the $LVCS_1$ that originates at O_{MT1}. Let the Z axis of $LVCS_1$ be represented as $\vec{O_{MT1}O_{OS}}$. Since both points O_{MT1} and O_{OS} are known, the unit vector along the Z axis is

$$\overrightarrow{Z_{MT1}} = \frac{(X_{OS}-X_{MT1})}{\text{Dist}_1}\vec{i} + \frac{(Y_{OS}-Y_{MT1})}{\text{Dist}_1}\vec{j} + \frac{(Z_{OS}-Z_{MT1})}{\text{Dist}_1}\vec{k} \quad (2)$$

where

$$\text{Dist}_1 = \sqrt{(X_{OS}-X_{MT1})^2 + (Y_{OS}-Y_{MT1})^2 + (Z_{OS}-Z_{MT1})^2} \quad (3)$$

The number of choices of orientations for the unit vectors along the X and Y axes is infinite. For ease of computation, we define the Y axis as parallel to the Y_WZ_W plane of the WCS. Since $\overrightarrow{Z_{MT1}}$ and $\overrightarrow{Y_{MT1}}$ are orthogonal, $\overrightarrow{Y_{MT1}}$ can be determined based on Eq. (2)

$$\overrightarrow{Y_{MT1}} = -\frac{(Y_{OS}-Y_{MT1})}{\text{Dist}_1'}\vec{i} + \frac{(X_{OS}-X_{MT1})}{\text{Dist}_1'}\vec{j} \quad (4)$$

where $\text{Dist}_1' = \sqrt{(Y_{OS}-Y_{MT1})^2+(X_{OS}-X_{MT1})^2}$. Finally, $\overrightarrow{X_{MT1}}$ is determined based on Eqs. (2) and (4)

$$\overrightarrow{X_{MT1}} = \overrightarrow{Y_{MT1}} \times \overrightarrow{Z_{MT1}} \quad (5)$$

Similarly, by applying Eqs. (2), (4), and (5) with a substitution of point O_{MT2} instead of O_{MT1}, the coordinate $LVCS_2$ can be determined.

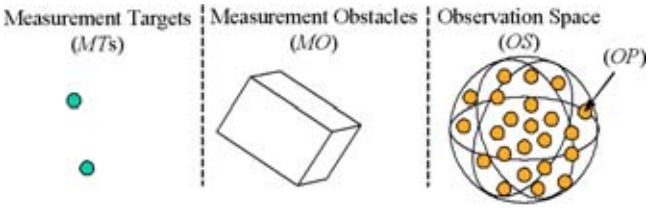

Fig. 9 Spherical representation of OS

3.2 Transformation of Local View Coordinate Systems to World Coordinate System. In Sec. 3.1, the local view coordinate systems for each measurement target (MT) as origin are determined. In this section, all the local view coordinate systems are transformed to coincide with the world coordinate system, and then all the visibility operations can be performed in a single coordinate system.

Each observation position (OP) has different coordinates in different coordinate systems. For example in Fig. 10, an OP is rep-

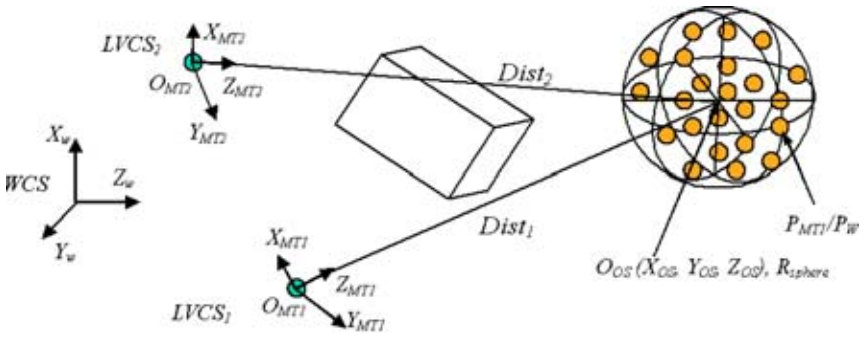

Fig. 10 Setup of local view coordinate system (LVCS) for different MTs

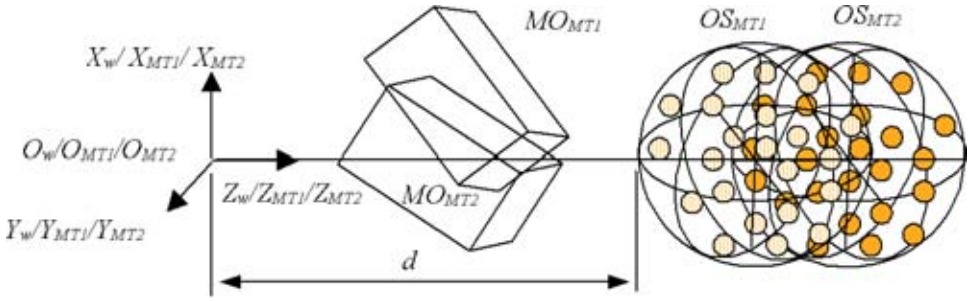

Fig. 11 Transformation from LVCS to WCS

resented as P_{MT1} and P_W in $LVCS_1$ and WCS, respectively. The relations between P_{MT1} and P_W can be defined by using the homogeneous transformations as follows:

$$P_{MT1} = R_{MT1} \cdot T_{MT1} \cdot P_W \tag{6}$$

where

$$R_{MT1} = \begin{bmatrix} \widehat{(X_{MT1})_x} & \widehat{(X_{MT1})_y} & \widehat{(X_{MT1})_z} & 0 \\ \widehat{(Y_{MT1})_x} & \widehat{(Y_{MT1})_y} & \widehat{(Y_{MT1})_z} & 0 \\ \widehat{(Z_{MT1})_x} & \widehat{(Z_{MT1})_y} & \widehat{(Z_{MT1})_z} & 0 \\ 0 & 0 & 0 & 1 \end{bmatrix} \text{ and}$$

$$T_{MT1} = \begin{bmatrix} 1 & 0 & 0 & -(O_{MT1})_x \\ 0 & 1 & 0 & -(O_{MT1})_y \\ 0 & 0 & 1 & -(O_{MT1})_z \\ 0 & 0 & 0 & 1 \end{bmatrix}$$

For each individual local view coordinate system, we maintain a copy of measurement obstacles (MO) and observation space (OS). Therefore, the number of copies is equal to the number of MTs. By applying homogeneous transformations as shown in Eq. (6), each LVCS can be transformed to be the WCS along with their corresponding copy of MOs and OS. Figure 11 illustrates the two local coordinate systems in a single world coordinate system, which coincide with each other. Two sets of MOs and OS, which correspond to $LVCS_1$ and $LVCS_2$, are shown in Fig. 11. It can be also observed that in $LVCS_1$ of Fig. 11, any obstacle MO whose Z coordinate is negative or greater than d is not a MO and can be eliminated from the list of MOs.

3.3 Screen Space Transformation in Each Local View Coordinate System. This step applies the SST in each individual local view coordinate system ($LVCS_i$ representing each MT_i) such that all the objects will be transformed from 3D to 2D space. This is a key step in simplifying the necessary computations. Since the OS work space has a spherical shape, all the parameters required to perform the SST are easy to calculate. Figure 12 shows all the necessary parameters for the SST conducted in the $LVCS_1$, which are summarized as follows (the used notation is explained in Fig. 7):

$$R_{sphere} = |X_{max}| = |X_{min}| = |Y_{max}| = |Y_{min}| \tag{7}$$

$$d = \text{Dist}_1 - R_{sphere} \tag{8}$$

$$f = \text{Dist}_1 + R_{sphere} \tag{9}$$

where Dist_1 can be obtained by using Eq. (3) and R_{sphere} is the radius of the spherical OS (Fig. 12).

Once all the parameters of SST transformation are determined, we can conduct the SST transformation for all the MOs and OPs in each individual LVCS (there is a set of MOs and OPs for each LVCS). Figure 13 illustrates MOs and OPs after the SST transformation in $LVCS_1$ and $LVCS_2$, respectively. Z values of all the objects in screen space can be omitted because all the lines of sight are parallel. Then we can obtain the models of MOs and OPs in the 2D coordinate as shown in Fig. 13. If an OP is covered by any MO, then in the original 3D view space the line of sight connecting corresponding MT and OP will be blocked by the MO, i.e., the MT is invisible to the OP. Since all MOs in view space are convex polyhedrons, all MOs are also convex polygons in the screen space [27]. This paper does not discuss the algorithm to identify if a point is covered by convex polygon because there is extensive literature in this area. A number of efficient methods are presented by Rourke [28].

In Sec. 3.2, all the local view coordinate systems have been transformed to coincide with the WCS as shown in Fig. 11. Therefore, all MOs and OPs in Fig. 13(*a*) and 13(*b*) can be considered as being allocated in one coordinate, which is shown in Fig. 14. Then we can see that in the original 3D view space the one set of MOs and OS become multiple sets in 2D screen space, each belonging to a single local view coordinate system, which corresponds to one MT. In Fig. 13, the two sets of MOs (MO_1 and MO_2) and OSs (OS_1 and OS_2) belong to $LVCS_1$ and $LVCS_2$, respectively.

3.4 Visibility Map and Visibility Matrix. In Sec. 3.3, the SST transformation is applied and, consequently, the visibility

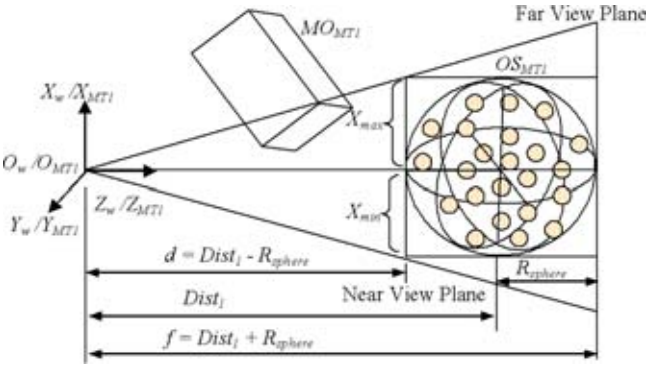

Fig. 12 Parameters for SST in $LVCS_1$

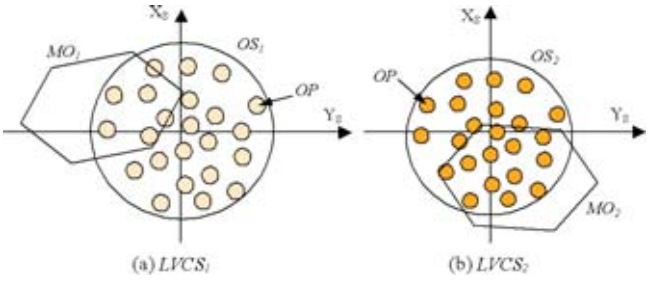

Fig. 13 SST in $LVCS_1$ and $LVCS_2$

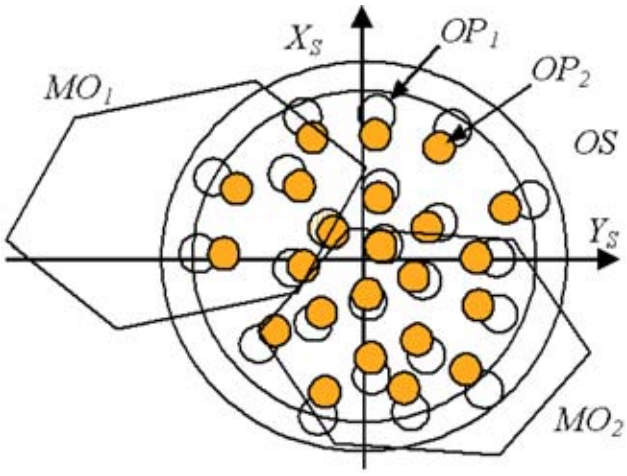

Fig. 14 Merged $LVCS_1$ and $LVCS_2$ systems into one WCS system

problem can be represented in 2D space, as has been illustrated in Fig. 14. It can be observed that there are two types of coordinate information represented in Fig. 14: information on measurement obstacles (MOs) and observation positions (OPs). In this section, translational operations are applied such that only information related to MOs needs to be maintained. Therefore, a simpler visibility map can be obtained, which can be further converted to an analytical form presented in the form of a visibility matrix. The visibility matrix will be used to solve the visibility problem in the Sec. 3.5.

Since the two sets of MOs and OPs in Fig. 14 are from the same set in the 3D view space, for any OP position in the view space we are always able to identify its transformations in $LVCS_1$ and $LVCS_2$, respectively. For example, in Fig. 15(*a*), P_{S1} and P_{S2} in the screen space are both transformed from the same observation position (P_W) in the view space, and then these two observation positions can be represented as follows based on Eqs. (1) and (6):

$$P_{S1} = T_{\text{pers-MT1}} R_{\text{MT1}} T_{\text{MT1}} P_W \tag{10}$$

$$P_{S2} = T_{\text{pers-MT2}} R_{\text{MT2}} T_{\text{MT2}} P_W \tag{11}$$

where P_w is an observation position in the original 3D view space, and other parameters are from Eqs. (1) and (6) and explained in Fig. 15(*a*).

In Fig. 15(*a*), if we translate P_{S1} and MO_1 so as to make P_{S1} coincide with the origin of the screen space coordinate, and then do the same translation to P_{S2} MO_2; the visibility map shown in Fig. 15(*b*) can be obtained with respect to a single OP position (P_w). Let V_V be an arbitrary vertex of the measurement obstacle in the view space, and its transformations in $LVCS_1$ and $LVCS_2$ are represented as V_{S1} and V_{S2} on MO_1 and MO_2, as shown in Fig. 15(*b*). Then we can deduce the following based on translation and Eqs. (10) and (11):

$$V_{S1} = T_{\text{pers-MT1}} R_{\text{MT1}} T_{\text{MT1}} (V_V - P_W) \tag{12}$$

$$V_{S2} = T_{\text{pers-MT2}} R_{\text{MT2}} T_{\text{MT2}} (V_V - P_W) \tag{13}$$

The visibility map illustrated in Fig. 15(*b*) can be interpreted as follows: if MO_i does not cover the origin, then the corresponding MT_i is visible to the OP. Otherwise, the corresponding MT_i is invisible to the OP, where *i* is the index of MTs. For example, Fig. 15(*b*) is the visibility map for an observation position (P_W), where there are two sets of MOs (MO_1 and MO_2) corresponding to MO_1 and MO_2, respectively. Since both MOs do not cover the origin, MT_1 and MT_2 are visible to the observation position P_W.

Figure 15(*b*) is a visibility map for just one OP position. By using the same procedure, the visibility maps for all OPs can be obtained. Then an overall visibility map can be presented as illustrated in Fig. 16. The evaluation of visibility is just to check if the MOs cover the origin or not. If 1 represents "visible" and 0 indicates "invisible," then the overall visibility map in Fig. 16 can be converted to a visibility matrix described in Table 2.

Two observation positions P_1 and P_2 (Fig. 16) are used as examples to explain the conversion from visibility map to visibility matrix. In Fig. 16, both MO_1 and MO_2 corresponding to P_1 do not cover the origin, so in the visibility matrix of Table 2, the values of the elements that are between P_1 and MT_1 and MT_2 are set to 1. For the MOs of P_2, MO_1 covers the origin but MO_2 does not. So the value of the element that is between P_2 and MT_1 is set to 0, and the value of the element that is between P_2 and MT_2 is set to 1. By using the same method, all the elements of the visibility matrix can be filled out.

3.5 Visibility of Observation Position Sets. Based on the visibility map and visibility matrix developed in previous sections, an algorithm is presented that identifies the minimum number of observation points through which all the measurement targets are visible to the measurement equipment.

From the SST-based visibility map, for any given OP, its vis-

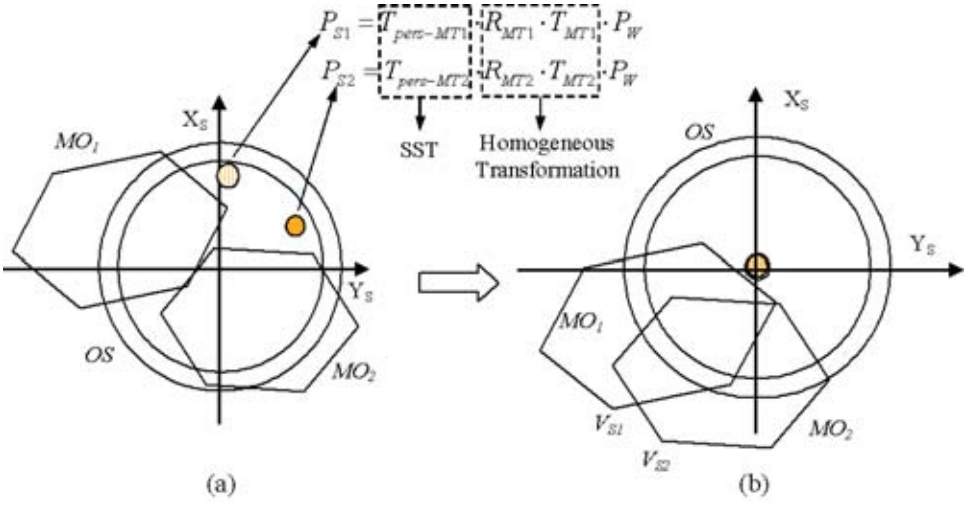

Fig. 15 Translation of moving the observation positions to coordinate origin

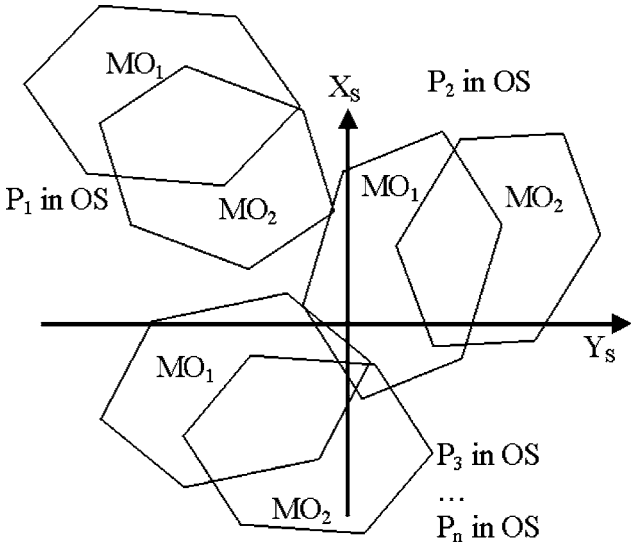

Fig. 16 Visibility map for all the OPs

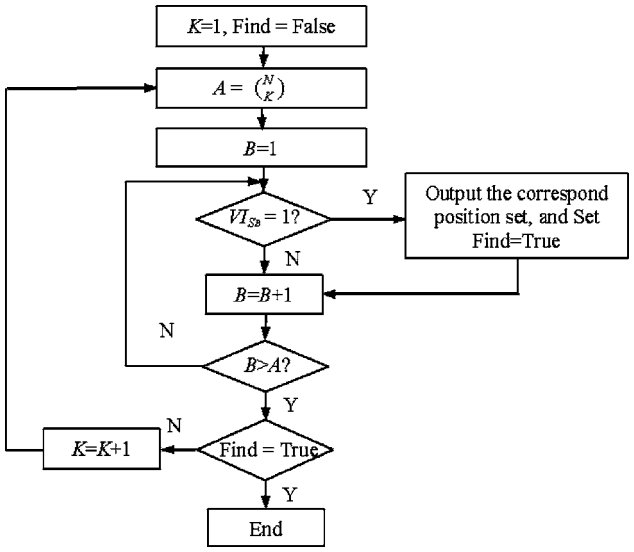

Fig. 17 Process of identifying the minimum number of setups for ME

ibility to all the MTs can be identified and can be represented as in Table 2. This general matrix represents the visibility of n OPs for m MTs subject to a given set of MOs. For the application of in-line fixture calibration, the ME should be able to measure all the MTs (all tooling elements); therefore, we need to develop an algorithm that can represent the visibility from a single OP to all the MTs. Let us define each row of the visibility matrix as a visibility code (VC), which is an m-bit binary code, corresponding to each OP. For example, in Table 2, the visibility code of P_1 is 11, which indicates that both MT_1 and MT_2 are visible to P_1.

Based on the visibility code of single OP, we extend it for a set of OPs. Assume $\boldsymbol{S}$ is a set of OP positions consisting of $P_1, P_2, \ldots, P_k$, and their visibility codes are $VC_{P1}, VC_{P2}, \ldots, VC_{Pk}$, respectively, then the visibility code of the set S is defined as

$$VC_S = VC_{P1} | VC_{P2} | \cdots | VC_{Pk} \tag{14}$$

where | is a "Bit OR" operation. For example, if $VC_{P1}=0001$, $VC_{P1}=1110$, then the visibility code of the point set $\{VC_{P1}, VC_{P1}\}$, represented as $VC_{\{P1,P2\}}$ is equivalent to 1111.

In order to identify whether an OP (or a set of OPs) is visible to all the MTs or not (this is a paramount requirement for fixture calibration), we define a visibility index (VI) based on the visibility code as follows:

$$VI = \begin{cases} 1 & \textit{if } VC/(2^m - 1) = 1 \\ 0 & \text{otherwise} \end{cases} \tag{15}$$

Equation (15) means that if all the bits of the visibility code are 1, then its visibility index is 1, otherwise, its visibility is 0. The visibility code and visibility index allow identification of the visibility for both a single OP position and for a set of OPs. If there is no single OP whose visibility index is 1, we need to identify the visibility of a set of OPs. For example, let us assume that we have four MTs and there is not a single OP position that has the visibility of 1 (i.e., all MTs are visible from a single OP position). Furthermore, say that the visibility code of one OP is 0011, and the visibility code of the second OP is 1100. Thus, the overall visibility code of both positions (set of two OPs) is 1111, and consequently, the overall MTs visibility from the two OP positions is 1. However, in the above case we have two OP positions, and thus, one extra setup of the measurement equipment is needed since the ME has to be moved from one OP to another in order to measure all the MTs.

Table 2 Formulation of visibility matrix

	MT_1	MT_2	$\cdots$	MT_{m-1}	MT_m
P_1	1	1	$\cdots$	$\cdots$	$\cdots$
P_2	0	1	$\cdots$	$\cdots$	$\cdots$
P_3	1	1	$\cdots$	$\cdots$	$\cdots$
$\cdots$	$\cdots$	$\cdots$	$\cdots$	$\cdots$	$\cdots$
P_{n-1}	$\cdots$	$\cdots$	$\cdots$	$\cdots$	$\cdots$
P_n	$\cdots$	$\cdots$	$\cdots$	$\cdots$	$\cdots$

Let $P\{P_i, i=1,2,\ldots,n\}$ represent all the OPs in a given OS, S_B is a subset of P, and K is the cardinality of subset of S_B, i.e., represents the number of OPs in the $\boldsymbol{S_B}$. The objective of minimizing the number of setups for ME can be formulized as

Identify the $\boldsymbol{S_B}$ *set with the smallest cardinality number* K $(\min(K))$ *such that its visibility index* $VI_{S_B}=1$.

The procedure of achieving the above objective is described in Fig. 17. In this flowchart, N is the total number of OPs and B represents the consecutive index of the subset S_B. In the first iteration, $K=1$, which means we are identifying the visibility index for a single OP. The visibility index value is checked and if there is no single OP position with visibility equal to 1, then $K=K+1$ (i.e., S_B with two OP positions is considered for further visibility analysis). This process is conducted iteratively until the smallest subset S_B (whose visibility index is 1) is identified.

4 Simplified Modeling of Measurement Obstacles

Since the SST transforms the visibility problem from 3D to 2D space, the computation of basic operation can be reduced significantly. But if we want to alleviate the complexity of the algorithm, the models of measurement obstacles need to be simplified, which reduces the number of computing iterations. In Secs. 4.1 and 4.2, a method of simplifying measurement obstacles is presented by which the complexity of the algorithm can be lessened.

4.1 Measurement Obstacles Simplification by Identification of the Boundaries. In Fig. 18, the MO is a convex polyhedron in the view space and E is its perspective projection on a projection plane P from the MT (i.e., E is a projection of edge chain $e_1e_2e_3e_4e_5e_6$ of the MO to plane P). The selection of plane P can be arbitrary as long as projection directions of any of the projected points are not part of P. It can be observed that although a polyhedral MO is composed of a number of polygons, it is not

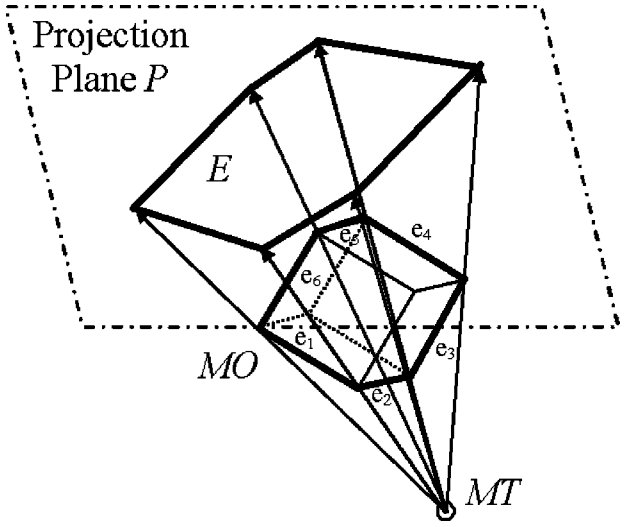

Fig. 18 Perspective projection of a convex MO from an MT

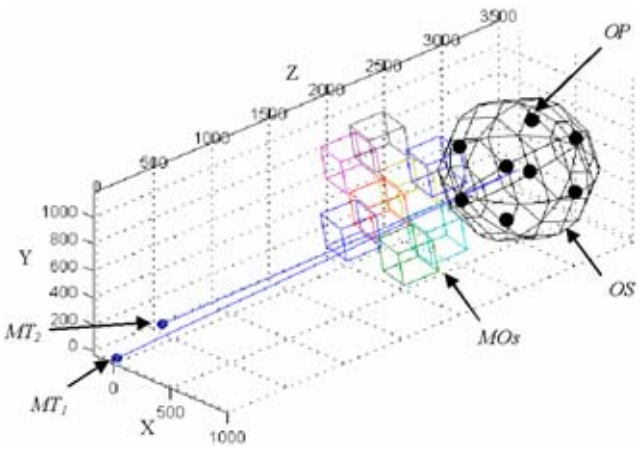

Fig. 20 Modeling of MTs, MOs, and OS

necessary to consider all these polygons as measurement obstacles. By identifying the "boundary" of the MO, for example, the edge chain $e_1e_2e_3e_4e_5e_6$ of the MO in Fig. 18, we can simply use one convex polygon (polygon E in Fig. 18) to represent the polyhedral MO in terms of its visibility.

In Fig. 19, the vector starting from the MT and ending at any point of the selected facet on the MO is represented by $\mathbf{N}$. For each facet, its normal vector toward the outside of the polyhedral MO is noted as $\mathbf{N}_F$. For a facet, if $\mathbf{N}_F \cdot \mathbf{N} > 0$, then it faces "toward" the MT. It is called a real obstacle (for example, facet F_1 in Fig. 19(a)). If $\mathbf{N}_F \cdot \mathbf{N} < 0$, the facet faces "away" from the MT, and it is hidden by real obstacles and has an impact on visibility. It is termed a pseudo-obstacle (for example, facet F_2 in Fig. 19(a)). By using this method, the pseudo-obstacles (facets) that do not contribute to the visibility can be identified and eliminated.

As discussed earlier, for a polyhedral MO, there is a boundary between real obstacles and pseudo-obstacles. For example, in Fig. 18, the edge chain $e_1e_2e_3e_4e_5e_6$ represents such a type of boundary for the hexahedral MO. In Fig. 19(b), for any edge e of a polyhedral MO, its two adjacent facets are represented as F_1 and F_2, respectively. If $\mathbf{N}_{F1} \cdot \mathbf{N}_1 < 0$ and $\mathbf{N}_{F2} \cdot \mathbf{N}_2 > 0$, or $\mathbf{N}_{F1} \cdot \mathbf{N}_1 > 0$ and $\mathbf{N}_{F2} \cdot \mathbf{N}_2 < 0$, i.e., the edge e is a transition between the real and pseudo-obstacles, then e is on the boundary dividing the real and pseudo-obstacles. By applying this verification for all the edges, the real visibility boundary of an obstacle can be identified. Then, the MO can be simply represented as a single convex polygon (the boundary) instead of a convex polyhedron. For example, in Fig. 18, the MO finally can be substituted with the convex

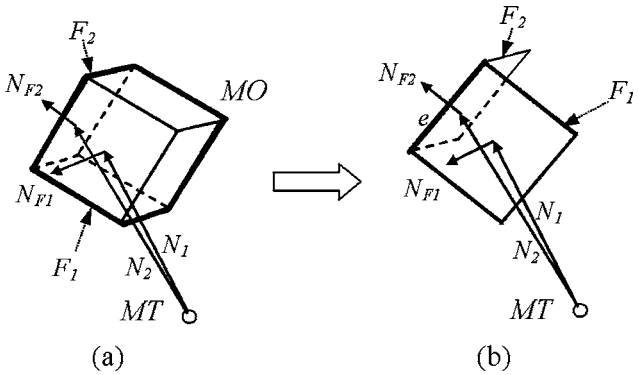

Fig. 19 Boundary identification of MO

polygon E. Since after the SST transformation, the polygon E is identical with the edge chain $e_1e_2e_3e_4e_5e_6$, we can just use the coordinate data of the edge chain $e_1e_2e_3e_4e_5e_6$ to conduct the SST transformation directly without transforming the MO to E. This also supports the transformation of MO using Eqs. (12) and (13), in which the V_V is one vertex on the boundary between real obstacles and pseudo-obstacles on the measurement obstacle.

4.2 Computational Complexity of the SST-Based Visibility Algorithm. Let us assume that m' is the number of MOs by using the simplified modeling of measurement obstacles, n refers to the number of discretized OPs inside of the OS, and k represents the number of MTs, then the complexity of this algorithm is $O(m'nk)$. Compared to the complexity of the DVA, which is $O(mnk)$, the only difference is m' instead of m. Since m represents the number of facets of all the convex polyhedrons and m' is the number of convex polygons (one convex polyhedron can be simplified as one convex polygon, illustrated in Fig. 18), i.e., the value of m' is much less than that of m, the complexity is reduced by using the simplified modeling of measurement obstacles.

5 Case Study

In this section, a case study presents the problem of a tooling calibration system with two MTs that need to be measured in the environment with eight cubic-shaped MOs, shown in Fig. 20. Since the purpose of this case study is to demonstrate the process of the proposed visibility algorithm, for simplicity, the spherical shape OS in this case is discretized into eight OP positions in which the measurement equipment can be located. A detailed discussion regarding the principle of discretizing an observation space into a number of observation positions is provided in Sec. 6.1.

Before applying the SST-based visibility algorithm, all the MO models need to be simplified to include only necessary geometries for visibility analysis. Figure 21 illustrates the MOs that have been simplified regarding MT_1 by using the method presented in Sec. 4.1. After the simplification process, a cubic obstacle can be presented by a number of closed spatial edges, which form a convex polygon in the screen space and have the same visibility as the original cubic obstacles.

Next the SST-based visibility algorithm is applied, and the procedure follows the steps presented in Sec. 3. Afterward, an overall visibility map for all OPs is obtained and shown in Fig. 22. Then the visibility can be evaluated based on the verification of whether the MOs cover the coordinate origin or not.

In order to illustrate the computed visibility map clearly, the visibility map in Fig. 22 is decomposed into eight visibility maps corresponding to the eight individual OPs. For example, Fig. 23 is

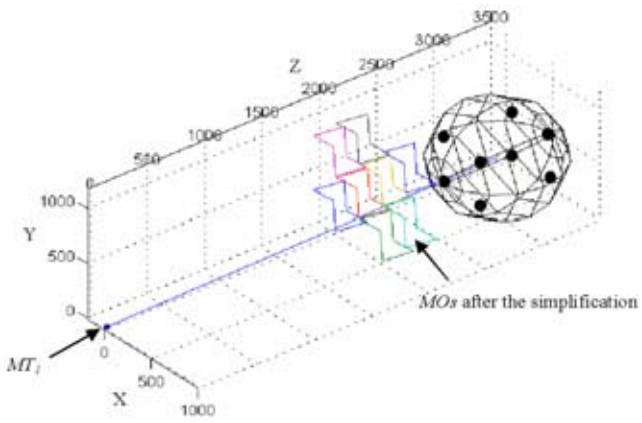

Fig. 21 Simplification of MOs regarding MT_1

the visibility map corresponding to OP_1, in which the dashed lines represent the MOs being observed from MT_1, and the solid lines represent the MOs being observed from MT_2. Since the coordinate origin is not covered by the two MOs, the visibility code of OP_1 is 11, which is further shown in a numerical form in Table 3. Following this approach, all the visibility maps for other OPs can

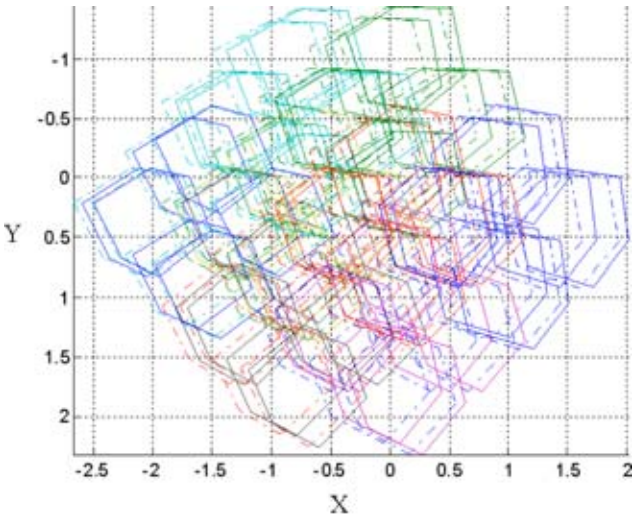

Fig. 22 Overall visibility map for all OPs

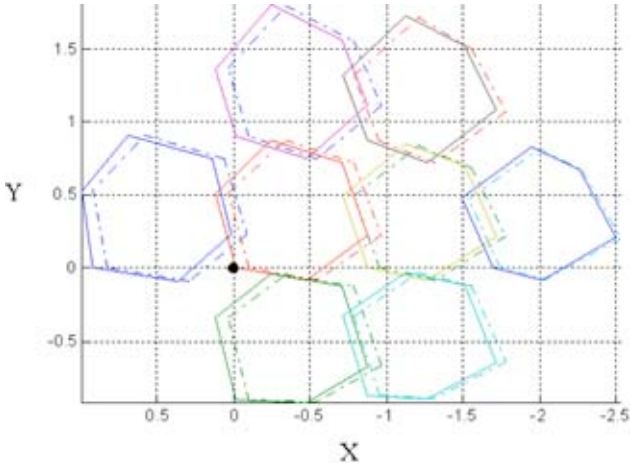

Fig. 23 Visibility maps corresponding to individual OP

Table 3 Visibility matrix obtained from the visibility map in Fig. 22

	MT_1	MT_2
OP_1	1	1
OP_2	1	1
OP_3	0	0
OP_4	0	0
OP_5	0	0
OP_6	0	0
OP_7	0	0
OP_8	1	1

be converted to the visibility matrix represented in Table 3. Finally, the visibility index of each OP can be determined, i.e., the visibility indices of OP_1, OP_2, and OP_8 are 1, and others have at least one 0. Therefore, if an ME is positioned to (is it "to" or "at") one of the positions: OP_1, OP_2, and OP_8, then both MT_1 and MT_2 can be measured without being blocked by any of the eight obstacles, signifying that only one setup is needed for the calibration of the presented system.

6 Discussions and Conclusions

6.1 Discretization of Observation Space. The case study in Sec. 5 illustrates the effectiveness of the proposed method. However, for practical applications, one critical issue should be addressed even before the SST method is applied, and that is, how to discretize the observation space to a set of observation positions. A schematic solution is provided below and detailed implementation will be given in a future paper.

Figure 24 is an example of a visibility map for one measurement target and three measurement obstacles. The basic principle for discretizing observation space is that the distribution of the discretized observation points must be dense enough to guarantee that the sightlines between measurement target and observation positions can go through the smallest gap that exists between measurement obstacles. In Fig. 24, the smallest gap between measurement obstacles is identified as δ (for more complex cases, for example where the gap shape is a polygon instead of a triangle, the computational techniques (such as triangulation of polygon) can be utilized to identify the smallest gap). For different measurement targets, the maps of measurement obstacles are different (illustrated by Fig. 13). Therefore, the smallest gap corresponding to each measurement target should be identified, among which the smallest one referred to as $\delta_{\min}$ will be used to discretize the

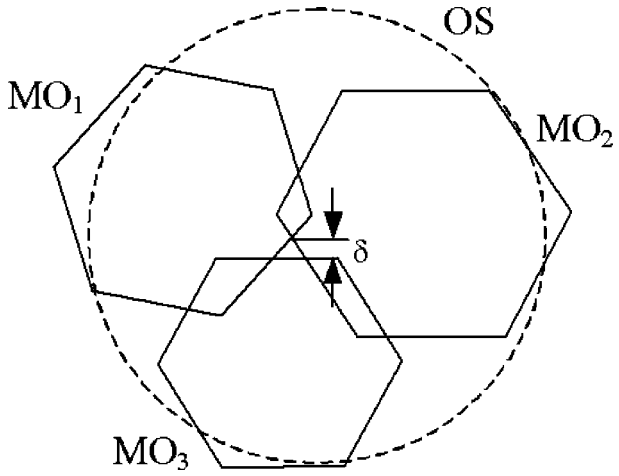

Fig. 24 Identification of minimum gap between MOs

observation space illustrated as OS in Fig. 24.

In 2D screen space, if an interval D_{dis} (which is the distance between adjoining observation points) is set to be equal to or less than $(2\sqrt{2}-\sqrt{6})\approx 0.378$ times of the smallest gap δ_{min}, then observation positions can be distributed to every gap between the measurement obstacles in 2D screen space (see Appendix for proof). By applying the inverse transformation of the screen space transformation (Eq. (1)), the distance D_{dis} in screen space can be transformed to the distance D'_{dis} in 3D view space. Consequently, the discretization of the observation space can be solved by distributing the observation positions uniformly using the obtained distance D'_{dis}.

Because of the utilization of the smallest gap (Fig. 24), the aforementioned method is actually a worst-case scenario. In practice, we can apply a "resampling" discretization approach to improve efficiency. At the beginning, a very sparse discretization is initialized. If the required visibility solution has not been found, eventually, the density of discretization will be increased until the density corresponding to the smallest distance (D'_{dis}) is reached. During this process, when resampling the observation points, the previous sampled points are still valid. By this approach, the distribution of the observation positions is able to catch any gaps between measurement obstacles, thereby, improving the computational efficiency.

6.2 Conclusion and Potential Applications. The calibration of assembly fixtures is critical for product quality. In order to reduce lead time of fixture calibration, the number of necessary setups for measurement equipment needs to be minimized. This paper clearly demonstrates the difference between various visibility problems. Focusing on the application of in-line fixture calibration that belongs to the environment-focused visibility problem, it presents a screen space transformation-based visibility algorithm, which converts the visibility problem from 3D to 2D space, such that the visibility operation is simplified significantly. Also a simplified modeling of measurement obstacle effectively reduces the computational complexity. Therefore, the proposed methodology is quite efficient. The provided case study validates the proposed method.

The methodology presented in this paper assumes that a complete computer-aided design (CAD) model of the production line is given and then the visibility algorithm can be executed to determine the best observation positions for measurement equipment. Under the circumstance in which only an incomplete CAD model is available, the proposed method can still provide a guideline by which the process designer can decide where to place various tooling or accessories, such as the controller cabinet, cable, etc., which are not included in the CAD model.

In our opinion, the SST-based visibility methodology can also be applied in various measurements and communications of multiple-target positions. The methodology, if used together with laser tracker or theodolite measurement systems, can be applied for production transfer line installation and calibration, installation of machine tools, the in-line aircraft assembly process, and other related fields. Additionally, the SST-based visibility methodology can also be applied for analysis and optimization of AGVs, robots navigation system, and building security.

Acknowledgment

The authors gratefully acknowledge the financial support of the API Inc., State of Wisconsin″s Industrial & Economic Development Research Program (I&EDR), the NSF Engineering Research Center for Reconfigurable Manufacturing Systems (NSF Grant No. EEC95-92125), and the National Science Foundation award DMI- 0218208.

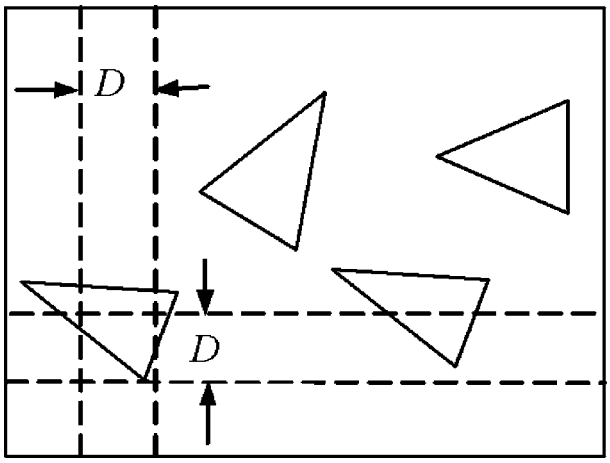

Fig. 25 Sampling interval on 2D plane

Appendix

Definition 1: Interval D is a valid sample interval if a 2D plane with a number of triangles on it is evenly sampled by using this interval (Fig. 25) such that there exists at least one sampling point in each triangle on the plane.

Lemma 1: For any triangle, its smallest height is referred to as h, there always exists a square with edge length equal to $2(2-\sqrt{3})h$, which is completely within the triangle (without any intersection with the edges of the triangle).

Theorem 1: Assume that there are a number of triangles on a plane, amid the heights of all the triangles, the smallest one is referred to as h. Any sampling interval D that satisfies $D\leqslant(2\sqrt{2}-\sqrt{6})h$ is a valid sampling interval.

Proof of lemma 1: This proof follows two steps: (i) for equilateral triangles, the lemma holds, and (ii) for any triangle with arbitrary shape, which is generated from an equilateral triangle, the lemma still holds.

Step 1: For an equilateral triangle ABC (Fig. 26) with height equal to h, its vertices can be represented as $A\left(-\frac{\sqrt{3}}{3}h,0\right)$, B $(h,0)$, and C $\left(\frac{\sqrt{3}}{3}h,0\right)$, $MQPO$ is an inscribed square of triangle ABC. The edge length of $MQPO$ can be calculated as $a=2(2-\sqrt{3})h$.

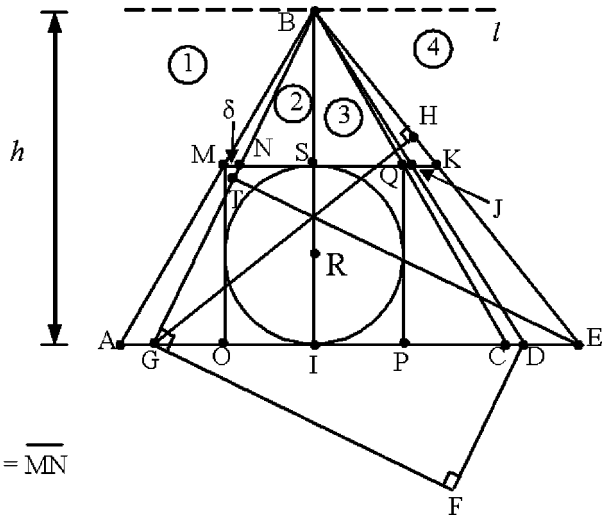

Fig. 26 Illustration of obtaining triangle with arbitrary shape from an equilateral triangle

Since the shortest height of the triangle can be represented by $\overline{BI}=h$, for equilateral triangles lemma 1 holds.

Step 2: For any other general case other than equilateral triangle, which takes *BI* as the shortest height (Fig. 26), we can generate it by rotating the edges of the corresponding equilateral triangle.

In Fig. 26, the straight lines *l*, *BA*, *BI*, and *BC* divide the half plane into four sectorial areas, which are represented as area 1, 2, 3, and 4. For a triangle with any arbitrary shape, it can be obtained by taking *B* as one vertex and *BI* as one of its heights, keeping the bottom line of the triangle passing through OP and rotating *BA* and *BC*. There must be six cases that can be classified as follows:

1. Both *BA* and *BC* fall into area 1 and/or 2
2. Both *BA* and *BC* fall into area 3 and/or 4
3. *BA* falls into area 2(3) and *BC* falls into area 3(2)
4. *BA* falls into area 1(4) and *BC* falls into area 4(1)
5. *BA* falls into area 2 and *BC* falls into area 4
6. *BA* falls into area 1 and *BC* falls into area 3

In cases 1, 2, and 3, *BI* is no longer the shortest height, so these cases will not be considered. For case 4, it is easy to see that the lemma holds. Case 5 and 6 are essentially identical. We will prove that under case 5, the lemma holds.

In Fig. 26, first, rotating anti-clockwise *BA* around *B* and stopping at the position *BG* within area 2, in order to make the square *MQPO* within the triangle, *MQPO* must be translated to, at least, make *M* coincident with *N*. The length of MN is referred to as δ.

In order to still make *BI* the shortest height of the triangle, edge *BC* must be rotated, at least, to position *BD* (the distance from *D* to *BG* is $\overline{FG}=h$) or position *BE* (the distance from *G* to *BE* is $\overline{GH}=h$). Both *BD* and *BE* are within area 4.

Scenario 1: *BC* is rotated to *BD*. Since $\overline{SI}/\overline{BI}=2(2-\sqrt{3})$, we can get $\overline{MN}/\overline{AG}=\overline{BM}/\overline{BA}=1-(\overline{SI}/\overline{BI})=2\sqrt{3}-3=\mu$. Namely, $\overline{AG}=\delta/\mu$. Therefore, $\overline{IG}=\overline{IA}-\overline{AG}=\frac{\sqrt{3}}{3}h-(\delta/\mu)$. Since ΔGBI and ΔDGF are identical, it is easy to see $\overline{GF}=\overline{BI}=h$ and $\overline{DF}=\overline{GI}=\frac{\sqrt{3}}{3}h-(\delta/\mu)$. Consequently, we can obtain

$$\overline{GD}=\sqrt{\overline{GF}^2+\overline{DF}^2}=\sqrt{\frac{4}{3}h^2+\frac{\delta^2}{\mu^2}-\frac{2\sqrt{3}}{3}\frac{h\delta}{\mu}}$$

and then, because $\overline{GC}=\frac{2\sqrt{3}}{3}h-(\delta/u)$, we get

$$\overline{CD}=\overline{GD}-\overline{GC}=\sqrt{\frac{4}{3}h^2+\frac{\delta^2}{\mu^2}-\frac{2\sqrt{3}}{3}\frac{h\delta}{\mu}}-\frac{2\sqrt{3}}{3}h+\frac{\delta}{u}.$$

Finally, *QJ* is obtained as

$$\overline{QJ}=\overline{CD}\cdot u=\mu\sqrt{\frac{4}{3}h^2+\frac{\delta^2}{\mu^2}-\frac{2\sqrt{3}}{3}\frac{h\delta}{\mu}}-\frac{2\sqrt{3}}{3}h\mu+\delta$$

Since $\delta<\overline{SM}$, we can obtain $\delta<\frac{\sqrt{3}}{3}h\mu$, based on, which it is easy to see, that $\overline{QJ}<\delta$.

Scenario 2: *BC* is rotated to *BE*. ΔGBI and ΔGET are homothetic triangles, and ΔGBI and δDGF are identical. Therefore, the following result holds:

$$\overline{GE}=\frac{\overline{GB}\cdot\overline{GT}}{\overline{GI}}=\frac{\overline{GD}\left(\frac{1}{2}\overline{GD}\right)}{\overline{GI}}=\frac{\frac{2}{3}h^2+\frac{\delta^2}{2\mu^2}-\frac{\sqrt{3}}{3}\frac{h\delta}{\mu}}{\frac{\sqrt{3}}{3}h-\frac{\delta}{\mu}}$$

and then $\overline{CE}=\overline{GE}-\overline{GC}=\delta^2/2\mu^2+\frac{\sqrt{3}}{3}h\delta/\mu/\frac{\sqrt{3}}{3}h-\delta/\mu+\delta/u$. Finally, we obtain *QK* as,

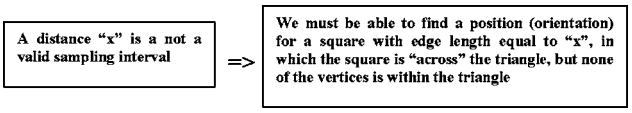

Fig. 27 Logic inference of the sampling interval

$$\overline{QK}=\mu\overline{CE}=\frac{\frac{\delta^2}{2}+\frac{\sqrt{3}}{3}h\delta\mu}{\frac{\sqrt{3}}{3}h\mu-\delta}+\delta$$

Since $\delta<\frac{\sqrt{3}}{3}h\mu$, it is easy to obtain that $\overline{QK}>\delta$.

Based on the aforementioned results of scenarios 1 and 2, we can get the following inequality:

$$\overline{QJ}<\delta<\overline{QK} \text{ or } \overline{CD}<\overline{CE}$$

In Fig. 26, for any triangle obtained by rotating edges *BA* and *BC* of triangle *ABC*, it is found that if keeping *BI* as the shortest height, *BA* and *BC* must be rotated to certain positions so that the other two heights ($\overline{GF}$ and $\overline{GH}$) are $\geqslant\overline{BI}$. From the results of scenarios 1 and 2, we can see that this condition can be satisfied only when *BC* is rotated to *BE* or beyond if *BA* is rotated to *BG*. At this moment, the two other heights are represented by $\overline{ME}$ and $\overline{GH}$. Since $\overline{ME}>\overline{GF}=h$, which is a result from $\overline{CD}<\overline{CE}$, and $\overline{GH}=h$, $\overline{BI}$ is still the shortest height of the triangle. Afterward, based on the aforementioned inequality, we know that $\overline{QK}$ is greater than $\overline{MN}$, which is defined as δ. Therefore, the square *MQPO* is still able to be within the triangle. Consequently, lemma 1 holds.

Proof of theorem 1: Based on definition 1, we can have the logic inference described in Fig. 27. The term "across" in the right side of the inference means partial or complete overlap. The scenario described in the right side of the inference can be illustrated by Fig. 28.

In Fig. 29, the square *DEFG* is obtained based on lemma 1; its edge length is $2(2-\sqrt{3})h$. Therefore, the inscribed circle *S* of square *DEFG* has a diameter of $2(2-\sqrt{3})h$. Furthermore, any inscribed square of circle *S* has a diameter of $(2\sqrt{2}-\sqrt{6})h$. Obviously, any inscribed square of circle *S* must be within the circumscribed square (*DEFG*) of circle *S*. Consequently, if we use the interval $D\leqslant(2\sqrt{2}-\sqrt{6})h$ to evenly sample the plane, it is impossible to find the scenario described by the right side of the aforementioned logic inference (Fig. 28). By applying contrary and inverse propositions of the logic inference (Fig. 27), we can con-

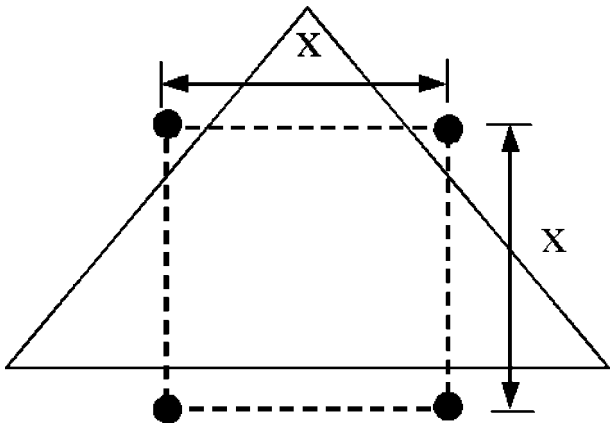

Fig. 28 Scenario of the invalid sampling interval

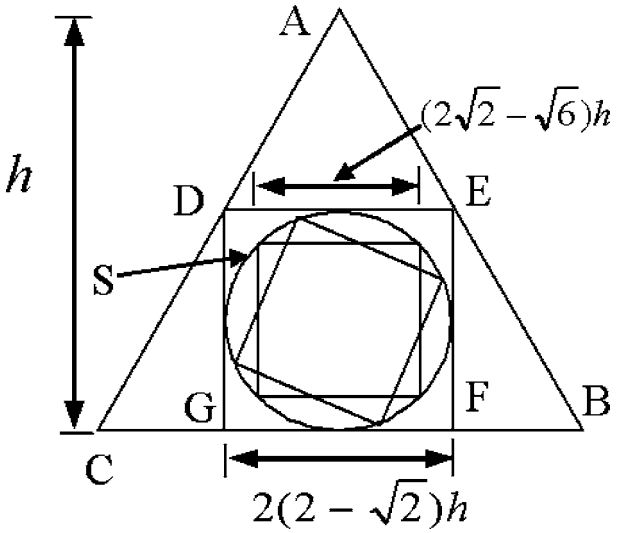

Fig. 29 Determination of the sampling interval

clude that any interval that satisfies $D \leqslant (2\sqrt{2}-\sqrt{6})h$ is a valid sampling interval. Therefore, theorem 1 is proved.

References

[1] Shalon, D., Gossard, D., Ulrich, K., and Fitzpatrick, D., 1992, "Representing Geometric Variations in Complex Structural Assemblies on CAD Systems," *ASME Advances in Design Automation*, ASME, New York, Vol. 2, pp. 121–132.

[2] Ceglarek, D., and Shi, J., 1995, "Dimensional Variation Reduction for Automotive Body Assembly," Manuf. Rev., **8**(2), pp. 139–154.

[3] Hu, S., and Wu, S. M., 1992, "Identifying Root Causes of Variation in Automobile Body Assembly Using Principal Component Analysis," Trans. NAMRI, **20**, pp. 311–316.

[4] Ceglarek, D., Shi, J., and Wu, S. M, 1994, "A Knowledge-Based Diagnostic Approach for the Launch of the Autobody Assembly Process," ASME J. Eng. Ind., **116**(4), pp. 491–499.

[5] Ceglarek, D., and Shi, J., 1996, "Fixture Failure Diagnosis for Autobody Assembly Using Pattern Recognition," ASME J. Eng. Ind., **118**(1), pp. 55–66.

[6] Apley, D. W., and Shi, J., 1998, "Diagnosis of Multiple Fixture Faults in Panel Assembly," ASME J. Manuf. Sci. Eng., **120**(4), pp. 793–801.

[7] Rong, Q., Ceglarek, D., and Shi, J., 2000, "Dimensional Fault Diagnosis for Compliant Beam Structure Assemblies," ASME J. Manuf. Sci. Eng., **122**(4), pp. 773–780.

[8] Ding, Y., Ceglarek, D., and Shi, J., 2002, "Fault Diagnosis of Multistage Manufacturing Processes by Using State Space Approach," ASME J. Manuf. Sci. Eng., **124**(2), pp. 313–322.

[9] Camelio, J. A., and Hu, S. J., 2004, "Multiple Fault Diagnosis for Sheet Metal Fixtures Using Designated Component Analysis," ASME J. Manuf. Sci. Eng., **126**(1), pp. 91–97.

[10] Koren, Y., Heisel, U., Jovane, F., Moriwaki, T., Pritschow, G., Ulsoy, G., and Brussel, H., 1999, "Reconfigurable Manufacturing Systems," CIRP Ann., **48**(2), pp. 527–540.

[11] Kong, Z., and Ceglarek, D., 2003, "Rapid Deployment of Reconfigurable Assembly Fixtures Using Workspace Synthesis and Visibility Analysis," CIRP Ann., **52**(1), pp. 13–16.

[12] Khan, A., Ceglarek, D., and Ni, J., 1998, "Sensor Location Optimization for Fault Diagnosis in Multi-Fixture Assembly Systems," ASME J. Manuf. Sci. Eng., **120**(4), pp. 781–792.

[13] Khan, A., Ceglarek, D., Shi, J., Ni, J., and Woo, T. C., 1999, "Sensor Optimization for Fault Diagnosis in Single Fixture System: A Methodology," ASME J. Manuf. Sci. Eng., **121**(1), pp. 109–117.

[14] Ding, Y., Kim, P., Ceglarek, D., and Jin, J., 2003, "Optimal Sensor Distribution for Variation Diagnosis in Multi-Station Assembly Processes," IEEE J. Rob. Autom., **19**(4), pp. 543–556.

[15] Djurdjanovic, D., and Ni, J., 2004, "Measurement Scheme Synthesis in Multi-Station Machining Systems," ASME J. Manuf. Sci. Eng., **126**(1), pp. 178–188.

[16] Huang, W., Kong, Z., Ceglarek, D., and Brahmst, E., 2004, "The Analysis of Feature-Based Measurement Error in Coordinate Metrology," IIE Trans., **36**(3), pp. 237–251.

[17] Chen, H. K., Hu, S. J., and Woo, T. C., 2001, "Visibility Analysis and Synthesis for Assembly Fixture Certification Using Theodolite Systems," ASME J. Manuf. Sci. Eng., **123**(1), pp. 83–89.

[18] http://www.apisensor.com

[19] http://www.imtecgroup.com

[20] Spyridi, A., and Requicha, A. A., 1990, "Accessibility Analysis for the Automatic Inspection of Mechanical Parts by Coordinate Measuring Machines," *Proc. of IEEE Int. Conf. of Robot Automation*, Cincinnati, IEEE, New York, pp. 1284–1289.

[21] Spitz, S., Spyridi, A. J., and Requicha, A. A., 1999, "Accessibility Analysis for Planning of Dimensional Inspection With Coordinate Measuring Machines," IEEE J. Rob. Autom., **15**(4), pp. 714–727.

[22] Spitz, S., and Requicha, A. A., 2000, "Accessibility Analysis Using Computer Graphics Hardware," IEEE Trans. Vis. Comput. Graph., **6**(3), pp. 208–219.

[23] Chen, L., and Woo, T. C., 1992, "Computational Geometry on the Sphere With Application to Automated Machining," J. Mech. Des., **114**(2), pp. 288–295.

[24] Woo, T. C., 1994, "Visibility Maps and Spherical Algorithms," Comput.-Aided Des., **26**(1), pp. 6–16.

[25] Wuerger, D., and Gadh, R., 1997, "Virtual Prototyping of Die Design Part Two: Algorithmic, Computational, and Practical Considerations," Concurr. Eng. Res. Appl., **5**(4), pp. 317–326.

[26] Yin, Z., and Xiong, Y., 2000, "Visibility Theory and Algorithms With Application to Manufacturing Processes," Int. J. Prod. Res., **38**(13), pp. 2891–2909.

[27] Watt, A., 2000, *3D Computer Graphics*, Addison-Wesley, Reading, MA.

[28] Rourke, J., 1998, *Computational Geometry in C*, Cambridge University Press, Cambridge, UK.